Atomic-scale mechanistic features of oxide ion conduction in apatite-type germanates†

Emma Kendrick,[a] M. Saiful Islam[b] and Peter R. Slater*[a]

Received (in Cambridge, UK) 31st October 2007, Accepted 28th November 2007
First published as an Advance Article on the web 17th December 2007
DOI: 10.1039/b716814d

Atomistic modelling studies of the apatite-type oxide ion conductor $La_{9.33}(GeO_4)_6O_2$ show that a key role of the O4 channel oxygen atoms appears to be as a reservoir for the creation of interstitial oxide ion defects, while the migration of these defects proceeds *via* the GeO_4 tetrahedra.

Apatite-type silicates and germanates, $La_{9.33+x}(Si/GeO_4)_6O_{2+3x/2}$, represent a new class of oxide ion conductors with potential applications as electrolytes for solid oxide fuel cells (SOFCs).[1–17] Isostructural with the well-known hydroxyapatite bioceramics, the silicates/germanates have been shown to exhibit high oxide ion conductivities exceeding those of yttria-stabilised zirconia, the traditional SOFC electrolyte.[12] Whereas the traditional fluorite- and perovskite-type oxide ion conductors conduct *via* oxide ion vacancies, the conductivity of these apatite systems is dominated by the transport of interstitial oxide ions, which can be either present as oxygen hyperstoichiometry ($x > 0$) or Frenkel defects.[4,9,10,12]

The structure of these materials is shown in Fig. 1, and can be described as comprising Si/GeO_4 tetrahedra arranged so as to form distinct oxide-ion and La channels running parallel to the *c* axis. In previous work we employed static lattice simulation techniques to investigate the mechanism of oxide ion conduction in the silicate system, $La_{9.33}(SiO_4)_6O_2$.[9] This work identified the most favourable interstitial oxide ion site to be at the periphery of the oxide ion channels, neighbouring the SiO_4 tetrahedra, subsequently confirmed by experiment.[10,12] The conduction mechanism was also investigated and predicted to follow a complex sinusoidal pathway, with an important feature being that the mechanism was aided by cooperative displacements of the silicate substructure, suggesting that the flexibility of the silicate substructure is essential to the observed high oxide-ion conductivities.

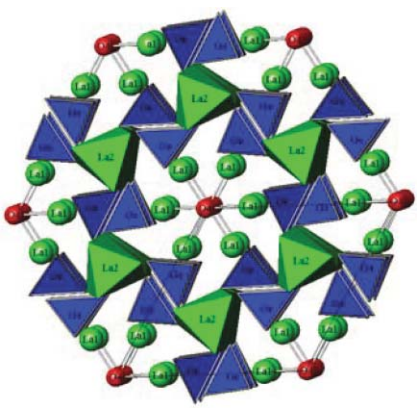

Fig. 1 The structure of $La_{9.33}(GeO_4)_6O_2$.

Combined simulation and structural (neutron diffraction, Extended X-ray Absorption Fine Structure (EXAFS)) studies have also helped to account for the influence of dopants on the conductivity of the silicate apatites,[15] in particular why small cation dopants (*e.g.* Mg) on the La site result in a reduction in the conductivity, while there is an enhancement for comparable doping on the Si site.[12,15] Similarly Bi doping (for La) significantly lowers the conductivity, which can be attributed to the lone pair of the Bi^{3+} atom blocking the conduction pathway.[12]

Recently we have been investigating the conductivities of the related germanate systems, $La_{9.33+x}(GeO_4)_6O_{2+3x/2}$, and have observed that in contrast to the silicates, they appear to be significantly less influenced by the nature of the dopant or the dopant site.[12] Thus high conductivities are observed even when small cations or Bi are substituted on the La site. This feature is somewhat surprising, and may indicate a range of conduction pathways, making the conductivity less sensitive to localized distortions.

In order to investigate this, we have extended our atomistic simulation work to cover an investigation of the germanium-based apatite, $La_{9.33}(GeO_4)_6O_2$. The description of the techniques employed will be brief, since more detailed descriptions are available elsewhere.[18] The atomistic simulation method utilises energy minimisation techniques to determine the lowest energy configuration of the crystal system with respect to the atomic positions. The potential energy of the crystal lattice is obtained by summing the long range Coloumbic terms and the short range repulsion and dispersion forces represented by well-tested Buckingham pair potentials.

An important feature of the model is the ability to describe the polarisation of the atoms and in this system the shell model was employed. The defects are modelled with the Mott–Littleton approach,[18] where the region around the defect is split into two regions. The relaxation of the inner region is calculated explicitly, while the atoms in the outer regions are relaxed by quasi-continuum methods.

The static lattice simulations were performed using the General Utility Lattice Program (GULP) code,[19] with the potentials fitted to experimental data on $La_{9.33}(GeO_4)_6O_2$ reported by Berastegui *et al.*,[16] with good agreement to the structure obtained. The

[a]*Chemical Sciences, University of Surrey, Guildford, GU2 7XH, UK. E-mail: p.slater@surrey.ac.uk; Fax: +44(0)1483 686851; Tel: +44(0)1483 686847*
[b]*Department of Chemistry, University of Bath, Bath, BA2 7AY, UK*
† Electronic supplementary information (ESI) available: experimental details. See DOI: 10.1039/b716814d

Buckingham potentials and shell charges used in the model are given in supplementary material, as is the comparison between calculated and experimental structures, showing good agreement.

With the establishment of a good structural model, a series of simulations were carried out on isolated point defects (vacancies and interstitials). The most favourable oxide ion vacancy position was determined to be at the O4 site in the central oxygen channel, in agreement with neutron diffraction observations.[10] The most favourable La vacancy site was found to be at the La site (La2) furthest from the oxygen channels, which also agrees well with the neutron diffraction data indicating that La vacancies occupy these sites.

In terms of the oxygen interstitial site, two equally favourable sites were located (Fig. 2): one was located at the edge of the channels neighbouring a GeO_4 unit (similar to that observed from our study of $La_{9.33}(SiO_4)_6O_2$ and found experimentally for oxygen hyperstoichiometric materials $La_{9.33+x}(Si/GeO_4)_6O_{2+3x/2}$[9,10]). The second position was found in between two GeO_4 units in adjacent channels. Although at first glance these appear to be completely different sites, the relaxed configurations are almost identical, emphasising the large intrinsic relaxation and structural flexibility in these apatite materials, as first shown from our earlier studies on $La_{9.33}(SiO_4)_6O_2$.[9] Thus the incorporation of an interstitial oxygen effectively creates a "Ge_2O_9" unit with two essentially five-coordinate Ge atoms with bond distances between 1.77 and 1.92 Å. In agreement with these modelling observations, the presence of five-coordinate Ge has recently been proposed from neutron diffraction studies by Pramana *et al.* on the oxygen excess system $La_{10}(GeO_4)_6O_3$.[17]

Using the calculated vacancy and interstitial defect energies, a series of Frenkel and Schottky defects were derived for $La_{9.33}(GeO_4)_6O_2$ (see supplementary information†). The key result is that the oxygen Frenkel defect is the most favourable with an energy of 2.94 eV (1.47 eV per defect), which is lower than for the apatite–silicate, $La_{9.33}(SiO_4)_6O_2$; the increased favourability of the interstitial site is consistent with the observation of higher oxygen excess compositions in the germanates.[12,15,17]

Following on from these defect calculations, the conduction pathway was investigated. To this end, an extensive search of the potential energy surface between adjacent vacancy and interstitial sites was undertaken. The activation energy for O4 oxide ion vacancy migration was determined to be 1.05 eV, with a pathway directly down the centre of the oxide ion channels. The most favourable interstitial oxide ion migration pathway was found to be down the centre of the GeO_4 groups following a "fan-like" pathway (Fig. 3): in this case a lower activation energy of 0.79 eV was determined. Both activation energies compare well with the experimentally determined conductivity value of 0.94 eV (see

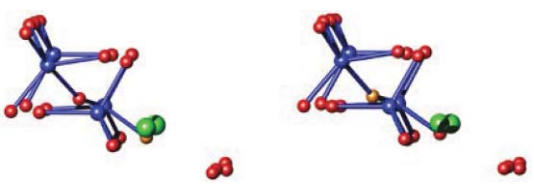

Fig. 2 Incorporation of an interstitial oxide ion (O5: orange) at the periphery of the O4 oxide ion channel (left) and between two adjacent GeO_4 tetrahedra (right). (Blue = Ge, red = O, green = La.)

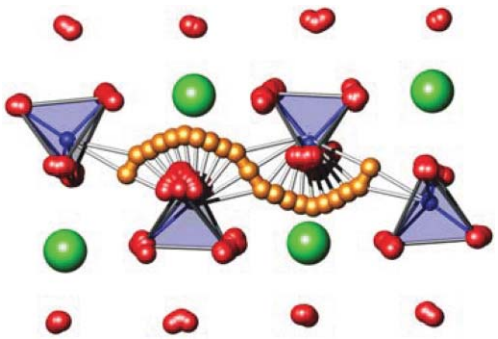

Fig. 3 Oxygen diffusion pathway *via* a "fan-like" mechanism along the *c* axis down the centre of the GeO_4 tetrahedra in $La_{9.33}(GeO_4)_6O_2$. The conduction process is aided by significant lattice relaxation, particularly of the GeO_4 tetrahedra.

supplementary information†), suggesting that both mechanisms could contribute to the oxide ion migration; however for the oxygen excess germanates, $La_{9.33+x}(GeO_4)_6O_{2+3x/2}$ ($x > 0$), the higher interstitial oxide ion defect content suggests that the interstitial mechanism will dominate.

For the interstitial pathway, in particular, the local relaxation during the conduction process of the germanate tetrahedra is quite considerable. Thus as for the silicate apatites,[9] the tetrahedral (in this case GeO_4) units play an important part in the conduction process. Moreover, the identification that the interstitial oxide ion leads to the effective creation of a "Ge_2O_9" unit linking two adjacent channels provides a potential avenue for interstitial oxide ion migration between channels (*i.e.* conduction in the *ab* plane).

The complexity of the interstitial mechanism raises the likelihood that cooperative or correlated effects, including rotation of the tetrahedra, may also contribute to the conduction processes. However, it is difficult to model such features using conventional static lattice techniques and so molecular dynamics (MD) calculations were also performed. These simulations employed the program DL_POLY.[20] The MD simulations solve Newton's equations of motion for an ensemble of particles, in this case with periodic boundary conditions for the supercell of $La_{9.33}(GeO_4)_6O_2$. The same interatomic potentials were used as for the static lattice calculations. Repetition of the integration algorithm yields a detailed picture of the evolution of ion positions and velocities as a function of time. For the MD work, a $2 \times 2 \times 3$ supercell with no symmetry constraints was set up for $La_{9.33}(GeO_4)_6O_2$. This supercell contained a total of 8 La vacancies, which were located on the La2 site, in agreement with experiment. The lowest energy configuration was found to be for the La vacancies located furthest away from each other, and this configuration was then used for the MD calculations. Several temperatures ranging from 673 K to 1673 K were investigated and at each temperature an initial equilibration of 60000 steps with a step size of 0.0004 ps was performed. The NVT ensemble was used (with constant number of particles, constant volume and constant temperature) for 150000 steps, with an initial equilibration of 40000 steps.

A number of key points raised from the static lattice calculations were confirmed by these MD studies. Firstly the creation of interstitial defects at the periphery of the oxide ion channels can be clearly seen (Fig. 4). Secondly the "fan-like" mechanism for conduction along the *c* direction was also observed in the MD

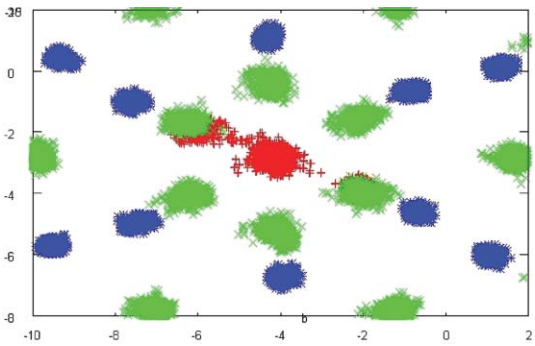

Fig. 4 The formation of an oxygen Frenkel defect by the promotion of an oxide-ion (red) out of the channel to a site at the channel periphery (La = green, Ge = blue), from the molecular dynamics (MD) simulations at 873 K.

simulations (see supplementary information†). However, the MD work also highlighted the complexity of the conduction processes in these apatite germanates. In particular, these studies showed that all the oxygen atoms, including those associated with the GeO_4 tetrahedra were mobile, the average migration activation energy in the range 873–1273 K being 0.98 eV, which reduces to 0.61 eV at higher temperatures. The former value agrees very well with the experimentally determined activation energy of 0.94 eV.

The role of the channel O4 oxide ions appears to be fundamentally as a "reservoir" for the creation of interstitial oxide ion defects as shown in Fig. 4; the higher MD activation energy for $T < 1273$ K may be related to this value involving both the formation of these defects as well as their migration. Once interstitial oxide ions are created, oxide ion migration then occurs *via* the GeO_4 tetrahedra, either *via* the fan-like mechanism along the *c* direction, or between adjacent channels (migration in the *ab* plane) by the formation and then breaking of the "Ge_2O_9" units; such processes are aided by the considerable relaxation of the structure around the interstitial oxide ion defects, as well as the rotational motion of the GeO_4 tetrahedra. It is worth noting that similar cooperative mechanisms for oxide-ion conduction have been recently found in gallium-based oxides with tetrahedral moieties.[21] It is clear from the trajectory plots that there is significant conduction perpendicular to *c*, showing that the conduction mechanism is more isotropic (3D) in nature (see supplementary information†), rather than being anisotropic, dominated by conduction along the *c* axis (1D pathway) as reported for the silicates. These findings of a range of conduction pathways are consistent with the experimental observations of the reduced influence on the oxide ion conductivity of Mg and Bi dopants on the La site in apatite germanates, compared to the silicates.[12]

In summary, our simulation studies have helped us to gain unique atomic-scale insight into the oxide-ion conduction processes in apatite-type germanates. In particular, the role of the O4 channel oxygen atoms appears to be as a "reservoir" for the creation of mobile interstitial oxide ion defects. The migration of these interstitial defects occurs *via* the GeO_4 tetrahedra, which allows for conduction both parallel and perpendicular to the c direction.

Notes and references

1 S. Nakayama, H. Aono and Y. Sadaoka, *Chem. Lett.*, 1995, 431.
2 S. Nakayama, M. Sakamoto, M. Higuchi and K. Kodaira, *J. Mater. Sci. Lett.*, 2000, **19**, 91.
3 S. Tao and J. T. S. Irvine, *Mater. Res. Bull.*, 2001, **36**, 1245.
4 J. E. H. Sansom, D. Richings and P. R. Slater, *Solid State Ionics*, 2001, **139**, 205.
5 H. Arikawa, H. Nishiguchi, T. Ishihara and Y. Takita, *Solid State Ionics*, 2000, **136–137**, 31.
6 L. Leon-Reina, M. E. Martin-Sedeno, E. R. Losilla, A. Caberza, M. Martinez-Lara, S. Bruque, F. M. B. Marques, D. V. Sheptvakov and M. A. G. Aranda, *Chem. Mater.*, 2003, **15**, 2099.
7 E. J. Abram, C. A. Kirk, D. C. Sinclair and A. R. West, *Solid State Ionics*, 2005, **176**, 1941.
8 J. E. H. Sansom, L. Hildebrandt and P. R. Slater, *Ionics*, 2002, **8**, 155.
9 M. S. Islam, J. R. Tolchard and P. R. Slater, *Chem. Commun.*, 2003, 1486; J. R. Tolchard, M. S. Islam and P. R. Slater, *J. Mater. Chem.*, 2003, **13**, 1956.
10 L. Leon-Reina, E. R. Losilla, M. Martinez-Lara, M. C. Martin-Sedeno, S. Bruque, P. Nunez, D. V. Sheptyakov and M. A. G. Aranda, *Chem. Mater.*, 2005, **17**, 596; L. Leon-Reina, J. M. Porras-Vasquez, E. R. Losilla and M. A. G. Aranda, *J. Solid State Chem.*, 2007, **180**, 1250.
11 V. V. Kharton, A. L. Shaula, M. V. Patrakeev, J. C. Waerenborgh, D. P. Rojas, N. P. Vyshatko, E. V. Tsipis, A. A. Yaremchenko and F. M. B. Marques, *J. Electrochem. Soc.*, 2004, **151**, A1236.
12 J. E. H. Sansom, J. R. Tolchard, D. Apperley, M. S. Islam and P. R. Slater, *J. Mater. Chem.*, 2006, **16**, 1410; E. Kendrick, M. S. Islam and P. R. Slater, *J. Mater. Chem.*, 2007, **17**, 3104.
13 Y. Masubuchi, M. Higuchi, S. Kikkawa, K. Kodaira and S. Nakayama, *Solid State Ionics*, 2004, **175**, 357.
14 S. Celerier, C. Laberty-Robert, J. W. Long, K. A. Pettigrew, R. M. Stroud, D. R. Rolison, F. Ansart and P. Stevens, *Adv. Mater.*, 2006, **18**, 615.
15 E. Kendrick, J. R. Tolchard, J. E. H. Sansom, M. S. Islam and P. R. Slater, *Faraday Discuss.*, 2007, **134**, 181; J. R. Tolchard, P. R. Slater and M. S. Islam, *Adv. Funct. Mater.*, 2007, **17**, 2564.
16 P. Berastegui, S. Hull, F. J. Garcia-Garcia and J. Grins, *J. Solid State Chem.*, 2002, **168**, 294.
17 S. S. Pramana, W. T. Klooster and T. J. White, *Acta Crystallogr., Sect. B: Struct. Sci.*, 2007, **63**, 597.
18 "*Computer Modelling in Inorganic Crystallography*", ed. C. R. A. Catlow, Academic Press, San Diego,1997.
19 J. D. Gale and A. L. Rohl, *Mol. Simul.*, 2003, **29**, 291.
20 W. Smith and T. R. Forester, *J. Mol. Graphics*, 1996, **14**, 136.
21 E. Kendrick, J. Kendrick, K. S. Knight, M. S. Islam and P. R. Slater, *Nat. Mater.*, 2007, **6**, 871.